26-Nov-2020

Re: comments of Reviewers 1 and 3

Dear Ms Natascha Töpfer:

We would like to express our sincere gratitude to the editors and anonymous reviews for their time and effort in handling our manuscript **(npg-2020-8)** entitled **"An enhanced correlation identification algorithm and its application on spread spectrum induced polarization data".**
We would like to say thanks again sincerely to the editors and anonymous reviews for their time and effort spent in handing our paper, as well as providing us many constructive comments for improving very much the presentation and quality of this manuscript.
It is worth pointing out that the reviewers' comments and suggestions have really constructively helped us improve further the quality and presentation of the manuscript. In light of their inspiring comments and suggestions, we have revised the manuscript duly and carefully, and the specific responses to the reviewers are listed as below, with the corresponding revisions **highlighted in blue color** in the revised manuscript.

Sincerely,
Dr. Siming He
hsmfly1982@163.com

Responses to comments of Reviewer 1

We greatly appreciate your suggestions, and we hope our revisions have addressed your questions and made this manuscript better.

Comment 1. 1.show extracted measured spectra (i.e., the resulting "data" after noise removal and conversion to the frequency domain): |R(f)|, Phase(f).

Response.

We added Phase(f) to the experiment on synthetic SSIP data record. Figures 1 and 2 show the relative error of Phase(f) are calculated and compared at the three main frequencies when the noise RMS ranges from 0 to 0.9.

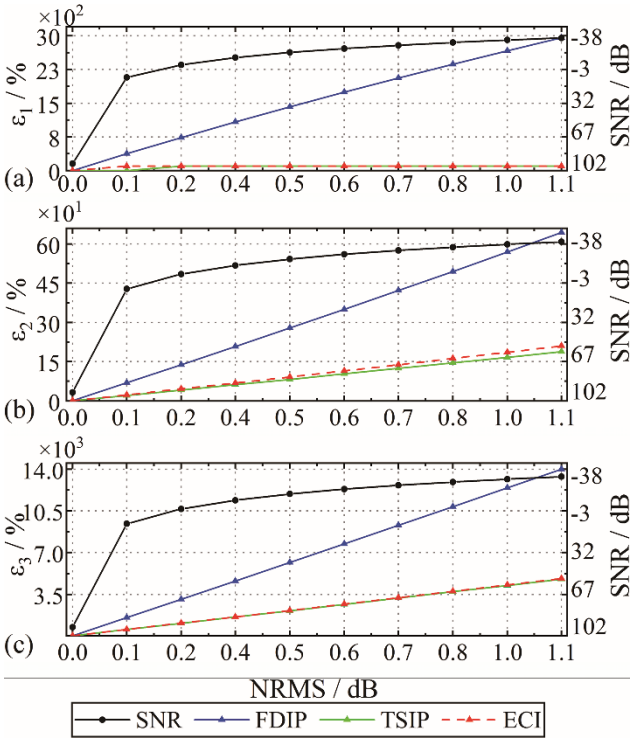

Figure 1. The effect of different degrees of Gaussian noise to the measures excitation signals in the phase-frequency characteristics. (a) SNR of the polluted potential signal. Complex resistivity relative error at (b) 80 Hz, (c) 160 Hz, (d) 320 Hz comparison using the three methods.

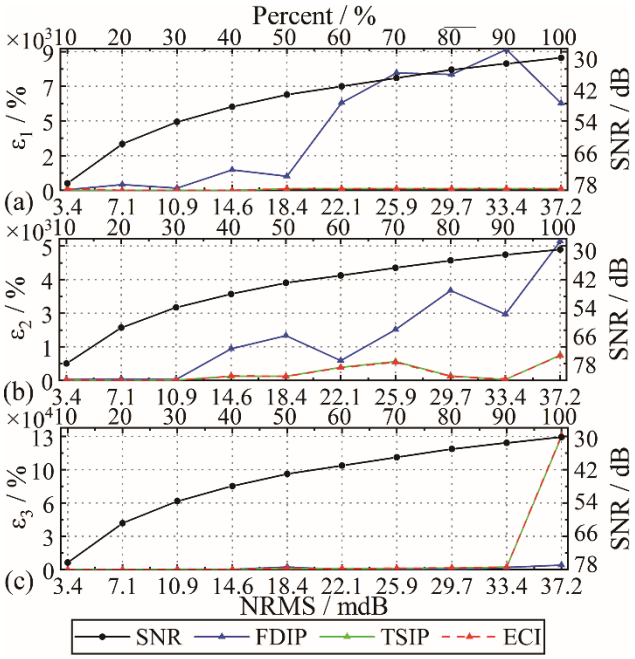

Figure 2. The effect of different levels of spike noises to the measured excitation signals. (a) SNR of the contaminated potential signal in the phase-frequency characteristics. Complex resistivity relative error at (b) 80 Hz, (c) 160 Hz, (d) 320 Hz comparison using the three methods.

From Figures 1 and 2, the results do not reflect the noise reduction performances of the three algorithms. Therefore, these results are not put into our manuscript. But |R(f)| and Phase(f) processed by three algorithms reflect their noise reduction performance well in the field experiment, as shown in Figure 3. So |R(f)| and Phase(f) in the field experiment are added to our manuscript.

This information is added on Page 9, line 16 and 17, Page 10, line 1 to 5 and Figure 3.

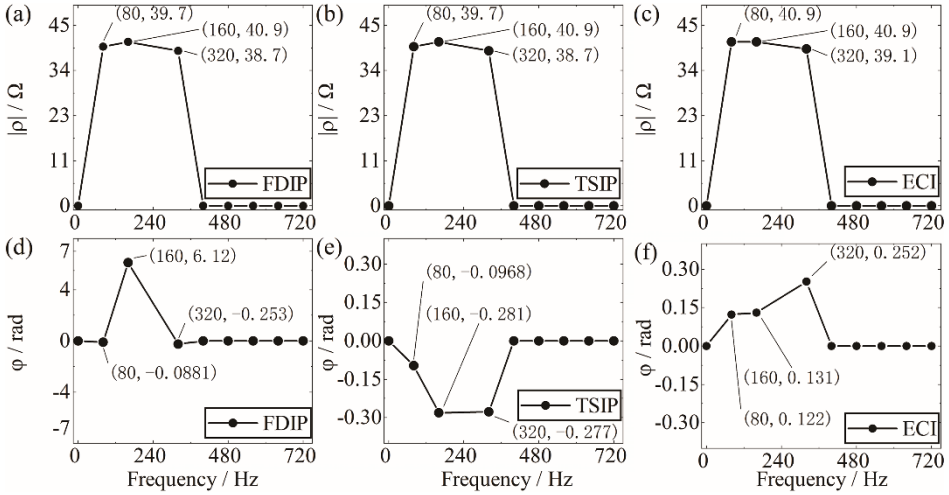

Figure 3. Complex resistivity spectrum calculated by the three algorithm (one period) in survey point No 21.

Comment 2. show phase results for the inversion results (if not easily included into the main text, additional magnitude/phase results for different frequencies could be supplied in a supplement)

Response.

The phase results for the inversion results given by Res2DInv software is shown as Figure 4. As we can see, this figure shows chaos information from the phase shift between $i(t)$ and $u(t)$ of the

three methods. This is because the loss layer surrounding the shelter is very weak polarized, so the phase shift is very small, which cause the result easily contaminated by some random factors. Therefore, we have not figured out how to extract meaningful information out of the phase results, but it is possible that with proper strong-polarized experiment field there could be different results. We are eager to explore that in our next experiment plan.

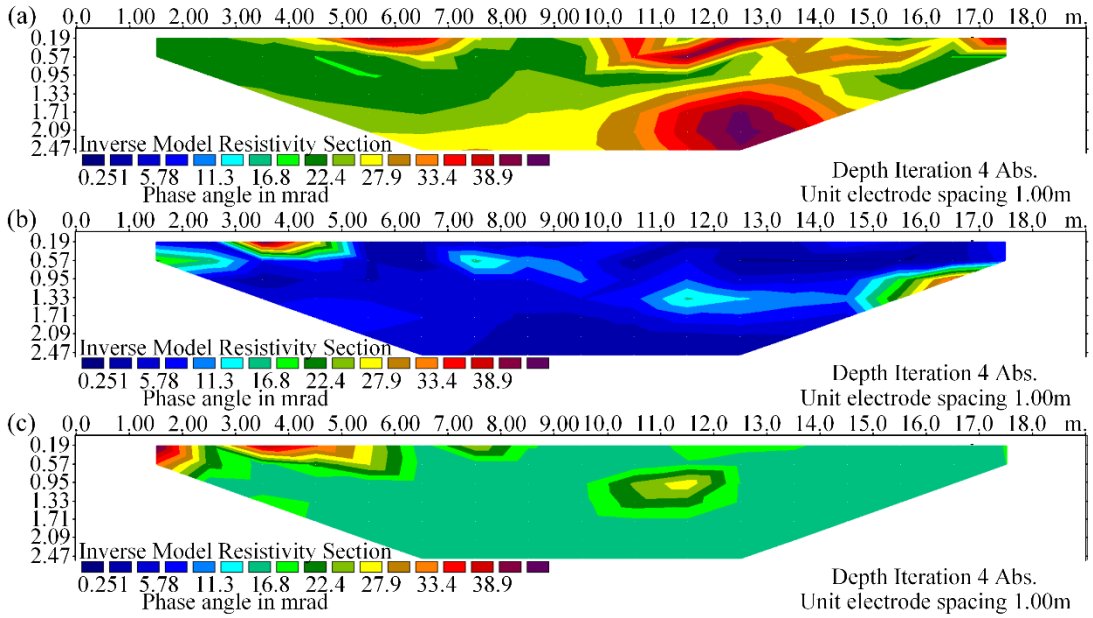

Figure 4. Inverted phase sections of the two high resistivity anomalies at 80Hz with using (a) the FDIP method, (b) the TSIP algorithm, and (c) the ECI algorithm.

Comment 3. Please employ a proper notation for complex entities. From my point of view most equations contain complex values.

Response.

We have modified some complex entities.

Page 4, line 19 to 23

Comment 4. page 4,line 17: "ZW-CMDSII" not defined - please provide a reference here as this seems to be related to the construction of a measurement system?

Response.

We have added reference the reference of ZW-CMDSII (Zhang, et al., 2014; He, et al., 2014;) to the paper.

Page 6, line 5 to 12

References

He, G. Wang, J. Zhang, B. Y. Li, M. and Ma, C.: Design of High-density Electrical Method Data Acquisition System, Instrument Technique and Sensor, 2014, 8, 18-19, https:// doi.org/10.3969/j.issn.1002-1841.2014.08.007.

Zhang, B. Y. He, G. and Wang J.: New High-density Electrical Instrument Measuring System. Instrument Technique and Sensor, 2014, 1, https://doi.org /10.3969/j.issn.1002-1841.2014.01.009.

Comment 5. page 4/ECI approach: My understanding of the main point of the ECI approach is that you assume uncorrelated noise for applied voltage (n1), measured voltage (n2), and measured injected current (n3) (otherwise the cross-correlations between those quantities shouldn't be zero, as stated in page 4, line 19). If this reading of mine is correct, I would like to see more discussion on this: Is this always the case? What about electronic noise (e.g., from the ADCs involved) - shouldn't this superimpose on all three noise components? I understand that this is probably not an issue here, but it would be nice if you could guide the reader into the right direction. Also, this main assumption should be more prominently presented in your manuscript.

Response.

What you understand is basically right. In our experiment, the applied voltage $u_{\mathrm{T}}(t)$ is measured within the powering system, so the environment interference only introduce noise into the measured voltage and measured infected current. In fact, $n_1(t)$ mainly consists of the floor noise of the measuring instruments (including ADCs noise), and very feebly influenced the coupling effect of $n_2(t)$ and $n_3(t)$, while $n_2(t)$ and $n_3(t)$ mainly consist of the environment noise. This is why we consider the cross-correlation between $n_1(t)$ $n_2(t)$ or $n_1(t)$ $n_3(t)$ 'approximately' zero. We adjust the expressions in page 4 line 13 to 15 to make it more clear. As for the electronic noise, since they are Gaussian noise, Figure 5 shows how its energy is compressed by the cross-correlation computation. But what you suggest inspires us to more thoroughly consider different noise sources. So we make further discussions on the correlation behaviors of these noise as below.

In a real environment, this model is contaminated by the environment interference and measuring instrument. It can be categorized into three types: the Gaussian random noise, the impulse interference, and the particular frequency disturbance (Wang and Li, 1986; Yan et al., 2016).

For our system, we assume the three noises are linearly overlapping on the three sensors, along with some weak influence of coupling effects. So, the noises in the three sensors are only different in amplitude. Hence,

$$n_1(t) = B_1 g(t) + C_1 p(t) + D_1 s(t) \tag{1}$$

$$n_2(t) = B_2 g(t) + C_2 p(t) + D_2 s(t) \tag{2}$$

$$n_3(t) = B_3 g(t) + C_3 p(t) + D_3 s(t) \tag{3}$$

where $n_k(t)$ is the noise in sensor Y_k, $k = 1,2,3$, respectively. $g(t)$, $p(t)$ and $s(t)$ are separately Gaussian random noise, impulsive noise and particular frequency interference. B_k, C_k and D_k are the amplitudes of $g(t)$, $p(t)$ and $s(t)$, $k = 1,2,3$, respectively.

According to the properties of the correlation function, the cross-correlation results of the three kind of noise is as below:

A. For the Gaussian random noise, when $-NT \le \tau \le NT$ and $\tau \ne 0$, $R_{gg}(\tau)$ is shown in Figure

5.

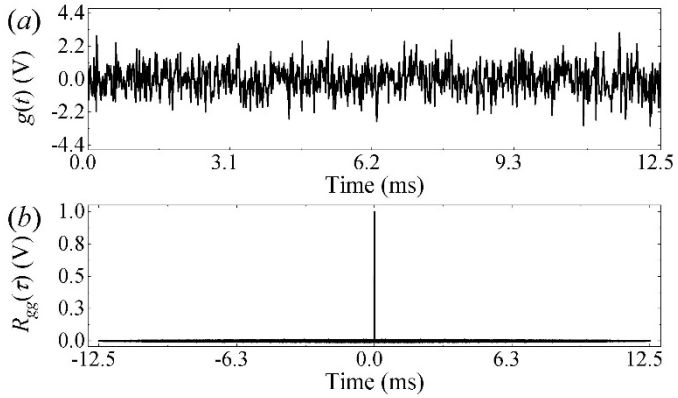

Figure 5. Waveform and autocorrelation for the Gaussian random noise $g(t)$. (a) its time domain waveform. (b) its autocorrelation $R_{gg}(\tau)$.

B. For the impulsive noise, when $-NT \le \tau \le NT$ and $\tau \ne 0$, it is considered that $R_{pp}(0) \gg R_{pp}(\tau)$, as shown in Figure 6.

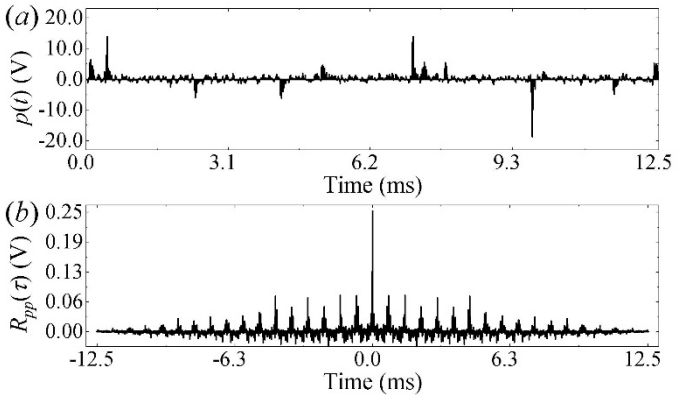

Figure 6. Waveform and autocorrelation for the impulsive noise $p(t)$. (a) its time domain waveform containing 20% of the outliers. (b) its autocorrelation $R_{pp}(\tau)$.

C. For the particular frequency disturbance, its autocorrelation has the same frequency with it, but when it is less effective for the transmitter output signal $u_{\mathrm{ab}}(t)$ than that of the $u_{\mathrm{mn}}(t)$ and $i(t)$, $D_1D_2R_{ss}(\tau)$ and $D_1D_3R_{ss}(\tau)$ can be effectively suppressed, as shown in Figure 7.

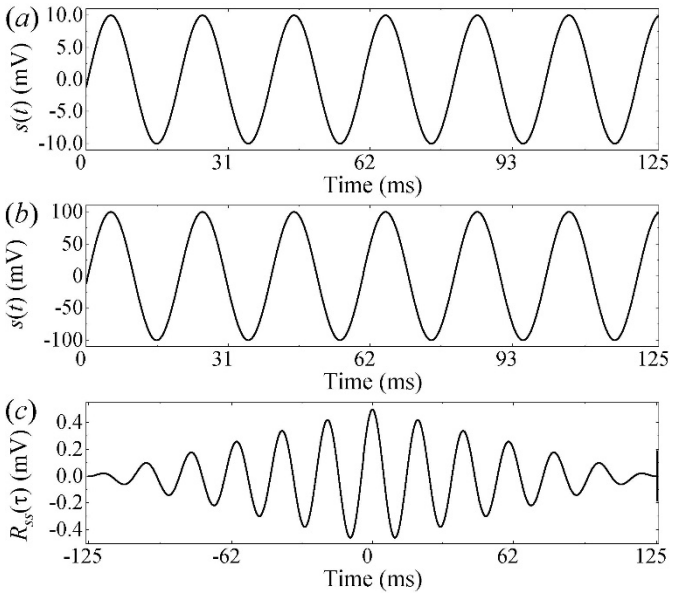

Figure 7. Waveform and autocorrelation for the particular frequency interference $s(t)$. The power-line interference (a) at $D_1 = 0.01$, (b) at $D_2 = 1$. (c) their cross-correlation $D_1 D_2 R_{ss}(\tau)$.

Based on the analysis above, it can be concluded that the influences of Gaussian random and impulsive noises are more effectively suppressed, while the particular frequency disturbance is attenuated to some degree when the noise is in lower intensity. Therefore, the proposed method has more value on denoising for Gaussian and impulsive random noises.

(2) In our experiment design, the noise sources and the system are considered independent and linearly superpositioned. Since our method demonstrates enhanced denoising ability to both kinds of noise, we think it is reasonable to say it has better denoising method. To further verify this assumption, we conduct an experiment on the denoising of mixed noises, as shown in Figure 8.

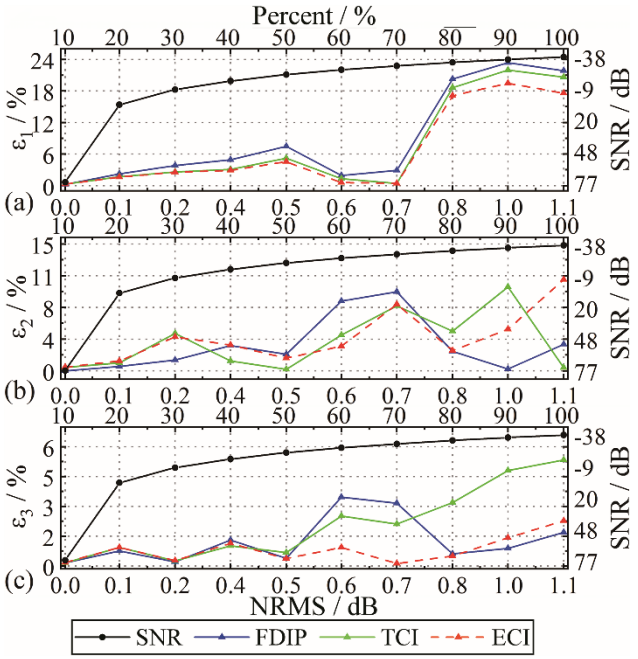

Figure 8. The injected current contaminated by simulated by sum of synthetic different degrees of Gaussian random noise and synthetic different levels of impulsive random noises, and RECR compared at three frequencies.

(a) SNR of the contaminated injected current. RECR at (b) 80 Hz, (c) 160 Hz, (d) 320 Hz comparison using the hybrid method and the others in the amplitude-frequency characteristics.

References

Wang, F.S., and Li, T., 1986, Industry of stray current resistivity observation and avoid interference distance: Northeastern Seismological Research, 2, 44–48. doi:10.13693/j.cnki.cn21-1573.1986.02.006

Yan, T. J., Wang, S. Q., Mang, Y. X., and Luo, X. Z., 2016, Influence of human interference on application of electrical prospect-ing and corresponding anti–interference measures , Mineral Exploration, 7, 634–639. doi:10.3969/j.issn.1674-7801.2016.04.016

Comment 6. Is NT specified? What interval was used for the synthetic and the experimental cases?

Response.

(1) NT is set 0.0125s in our experiment.

The information is added on Page 4, line 8 and Figure 4.

(2) The time interval is 0.0016ms, with sampling frequency of 625kHz.

Page 8, line 12

Comment 7. Fig 4: i(t) is the injected current, if I'm not mistaken. As such it should have a unit of Ampere, not Volts (same with the corresponding noise n3). If i(t) somehow has units of volts, please explain correspondingly (also in the previous text passages).

Response.

Thank you for pointing out our negligence. The relationship of the injected current signal between electrode A and electrode B is:

$$i(t) = u_i(t) / R_s , \tag{1}$$

where, R_s is a 1Ω sampling resistor, and $u_i(t)$ is the voltage at the sampling resistor.

Figure 4 is modified and the introduction is added on Page 5, line 10 to 14.

Comment 8. Synthetic case: It is not clear to me why you only add noise to the injected current and not to the measured voltage (n2) and the applied voltage (n1). Isn't that the whole point of your study? It would be nice if you could show that also for the synthetic case the cross-correlation of those noise components reduces to zero (p4, line19). I suppose this entails generating suitably uncorrelated random ensembles.

Response.

In our experiment the measurement line is 19m and in a stable environment, so we consider the system linear time-invariant and the noise from the current and voltage measurement are linearly superpositioned (Pelton, et al., 1983; De, et al., 1983; Vinegar and Waxman, 1984; De, et al., 1992; Garrouch and Sharma, 1998). Therefore, it is actually equivalent whether the noise is added to the injected current $i(t)$, the measured potential signal $u(t)$ or the applied voltage $u_T(t)$, the

equivalent relationship is described as below

(1) When the measured potential signal $u(t)$ and the injected current $i(t)$ are contaminated by the noise $n_2(t)$ and the noise $n_3(t)$, we can obtain

$$y_1=u_T(t)+n_1(t), \tag{1}$$

$$y_2=u(t)+n_2(t), \tag{2}$$

$$y_3=i(t)+n_3(t), \tag{3}$$

The cross-correlation functions can be expressed as follows:

$$R_{y_1y_2}(\tau)=R_{x_1x_2}(\tau)+R_{n_1n_2}(\tau), \tag{4}$$

$$R_{y_1y_3}(\tau)=R_{x_1x_3}(\tau)+R_{n_1n_3}(\tau), \tag{5}$$

Thus we can assume that the cross-relation between $n_1(t)$ and $n_2(t)$, $n_3(t)$ $R_{n_1n_2}(\tau)\approx 0$ and $R_{n_1n_3}(\tau)\approx 0$, we can further obtain:

$$R_{y_1y_2}(\tau)\approx R_{x_1x_2}(\tau) \tag{6}$$

$$R_{y_1y_3}(\tau)\approx R_{x_1x_3}(\tau) \tag{7}$$

(2) When the noise $n(t)$ from the current and voltage measurement are linearly superpositioned, $n(t)=n_1(t)+n_2(t)$ and the injected current $i(t)$ are contaminated by the noise $n(t)$, we can obtain

$$y_1=u_T(t)+n_1(t), \tag{8}$$

$$y_2=u(t), \tag{9}$$

$$y_3=i(t)+n(t)=i(t)+n_2(t)+n_3(t), \tag{10}$$

The cross-correlation functions can be expressed as follows:

$$R_{y_1y_2}(\tau)=R_{x_1x_2}(\tau), \tag{11}$$

$$R_{y_1y_3}(\tau)=R_{x_1x_3}(\tau)+R_{n_1n_2}(\tau)+R_{n_1n_3}(\tau), \tag{12}$$

Thus we can assume that the cross-relation between $n_1(t)$ and $n_2(t)$, $n_3(t)$ $R_{n_1n_2}(\tau)\approx 0$ and $R_{n_1n_3}(\tau)\approx 0$, we can further obtain:

$$R_{y_1y_2}(\tau)\approx R_{x_1x_2}(\tau) \tag{13}$$

$$R_{y_1y_3}(\tau)\approx R_{x_1x_3}(\tau) \tag{14}$$

Based on the analysis above, it can be concluded that Eq. (6) and Eq. (7) are consistent with Eq. (13)

and Eq. (14).This is why we only add noise on the injected current to represent the overall noise summation.

The cross-correlation results are shown in Figures 5 and 6 in response 5

References

Pelton, W. H., and Sill, W. R.: Interpretation of complex resistivity and dielectric data: Geophysical Transactions, 1983, 29, 297-330.

De Lima, O. A. L., and Sharma, M. M.: A generalized Maxwell‐Wagner theory for membrane polarization in shaly sands: Geophysics, 1992, 57, 431-440. doi:10.1190/1.1443257

Vinegar, H. J., and Waxman, M. H.: Induced polarization of shaly sands: Geophysics, 1984, 49, 1267–1287. doi:10.1190/1.1441755

Garrouch, A. A., Sharma M. M.: Dielectric dispersion of partially saturated porous media in the frequency range 10 Hz to 10 MHz: The Log Analyst, 1998, 39, 48-53.

Comment 9. While I think this step was taken to simplify the discussion, I think the simplification does not represent the problem at hand. As you stated in page 4, you also expect significant noise levels in n2 ("n2(t) and n3(t) may possess more massive energy..."), you should at least add suitable noise levels to n2 to test you algorithm. I still wonder why the current measurement entails such large noise components, given that this measurement is usually just a voltage measurement over a shunt resistor...

Response.

Sorry we did not put this clear enough in the manuscript. What we actually did was adding noise on the injected current to represent the overall noise summation in the system, as we explained in Response 8.

Since we consider our system as a linear time invariant system, whether the noise is added on the drive signal $u_T(t)$, the measured potential $u(t)$ or the current $i(t)$ are equivalent. When observing the field measured data, we found that the current signal is more heavily interfered by noise, as shown in Figure 1, so we decided to add noise on the supply current.

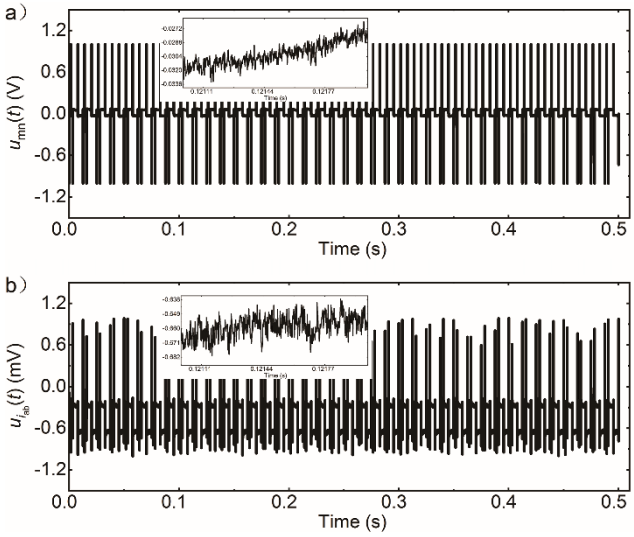

Figure 9. The time waveform of measured potential and supply current on electrode No. 53

Comment 10. Eq. 14/15: Is M defined in the text?

Response.

M is the length in the text as follows:

Page 5, line 12

Comment 11. Please use the same colorbar limits for all plots in Fig. 9. Otherwise a proper comparison is not possible.

Response.

Yes, we use the same colorbar limits for all plots in Figure 10 as follows:

Page 9, line 5

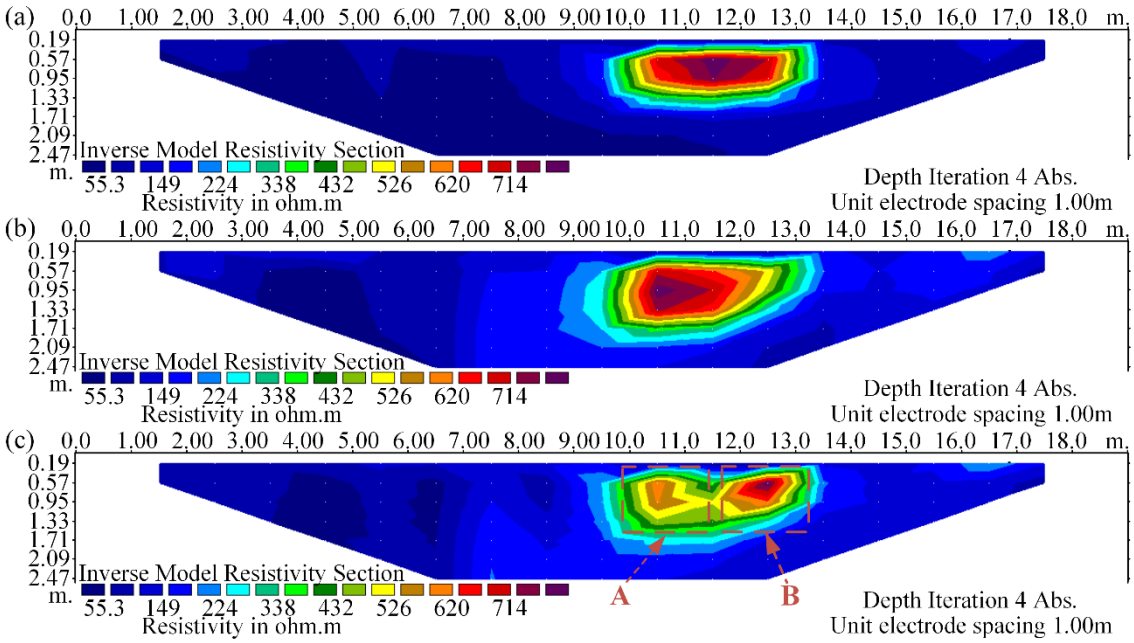

Figure 10. Inverted resistivity sections of the two high resistivity anomalies at 80Hz with using (a) the FDIP method, (b) the TSIP algorithm, and (c) the ECI algorithm.

Comment 12. the forward response of the final inversion model to the actual data. Does this analysis also follow the observed noise levels?

Response.

Sorry we are not so sure what you are referring to. In the actual field data, it is hard to extract the actual noise component. So we are trying to observe the noise level by calculating the SDs respectively, which help us evaluate the fluctuation degree of the processed signal, as shown in Figures 10 and 11.

As the figure shows, the ECI method has the lowest SD, which is why we deduce that our method has better denoising ability.

Page 9, and Page 10 line 1 to 6

Comment 13. Just to be sure (and perhaps encourage a slight extension of the last paragraph of the introduction to better clarify): The major point of this manuscript is that it takes into account also noise from the current measurement, which is not commonly done, right? For example Liu et al

2017, (10.1190/GEO2016-0109.1) seem to only assume noise on the primary potential measurements (The geophysics-paper also nicely shows pseudosections of both magnitude and phase - this would also be interesting here).

Response.

(1) In our field experiment, we did observe different noise levels both in potential and current measurements, in which the fluctuation in the current measurement is even acuter, as Figure. 11 shows.

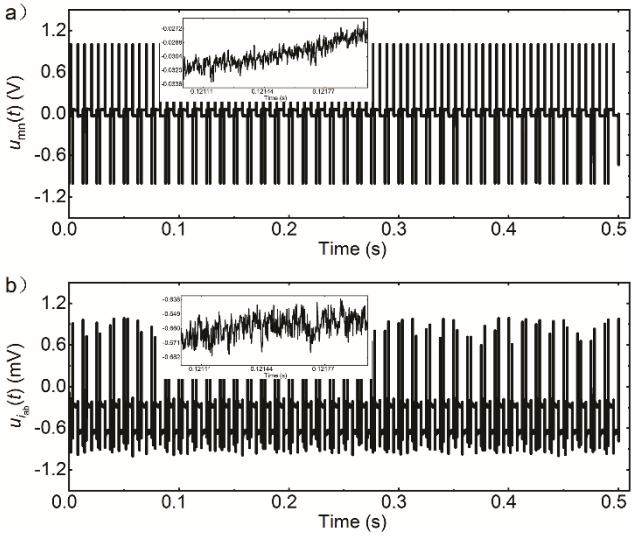

Figure 11. The time waveform of measured potential and supply current on electrode No. 53

(2) As stated Page 3, line 13 and 14, and Page 4, line 4 and 5 in our manuscript, that the denoising ability of the TSIP algorithm is limited is caused by that $i(t)$ is sensitive to $n_3(t)$. To solve this problem, the ECI algorithm is proposed. Therefore, that $i(t)$ is added noise to verify the noise reduction performance of the ECI algorithm.

(3) In fact, we think the it should represent the total noise summation in the system whether the noise component is added on the potential or current during calculation. From our understanding, the difference between us and Liu et al. is that they put this component in 'acquired potential U_0' (Eq. (5)), and we put it in I_{ab}. As we were trying to explain in response 8, this to operation should be equivalent during the cross-correlation process.

To clarify this, we added some explanations in the experiment section.

Page 5, line 17 and 24

Comment 14. In conclusion, I suggest to improve the presentation of the manuscript and to better work out the novel contribution of the ECI algorithm in comparison to the various other correlation-based noise-reduction algorithms out there, as well as to make sure your test cases compare to those of other studies (i.e., current and voltage noise).

Response.

As Liu. et al. mentioned, correlation noise-reduction algorithms applied on SSIP data processing is rarely reported, now all reported experiments we can find are Liu's research and 'Time-Domain Spectral Induced Polarization Based on Pseudo-random Sequence' (Li et al. 2013), as the TCI referring to in our manuscript. Liu's research is more of a screening method to find suitable signal sequence, rather than data processing method. Therefore what we can do is comparing our method with Mei Li's method. To be more accurate, we change 'TCI' to 'TSIP' when referring to Mei Li's

research in the manuscript.

Page2, line 3 and 4

Reference

Li, M. Wei, W. Luo, W. and Xu, Q: Time-domain spectral induced polarization based on pseudo-random sequence, Pure and Applied Geophysics, 170(12), 2257-2262, https://doi.org/10.1007/s00024-012-0624-z, 2013.

Responses to comments of Reviewer 3

We greatly appreciate your suggestions, and we hope our revisions have addressed your questions and made this manuscript better.

Comment 1. My general comment in that the results presented in manuscript are not discussed. Additionally, figure captions need to expand and explain the figure in a brief and simple way, so the reader doesn0t need to switch back to the tex to understand the figure.

Response.

(1) According to your suggestion, we have discussed the results.

Page 7, line 9 and 10

Page 9, line 16 and 17

Page 10, line 1 to 6

(2) According to your suggestion, we have modified the figure captions.

Page 6, line 2

Page 7, line 12

Page 9, line 6

Comment 2. I have read the first review of the manuscript, and I agree with the reviewer that it is essencial to show multi-frequency and phase data.

Response.

We added Phase(f) to the experiment on synthetic SSIP data record. Figures 1 and 2 show the relative error of Phase(f) are calculated and compared at the three main frequencies when the noise RMS ranges from 0 to 0.9.

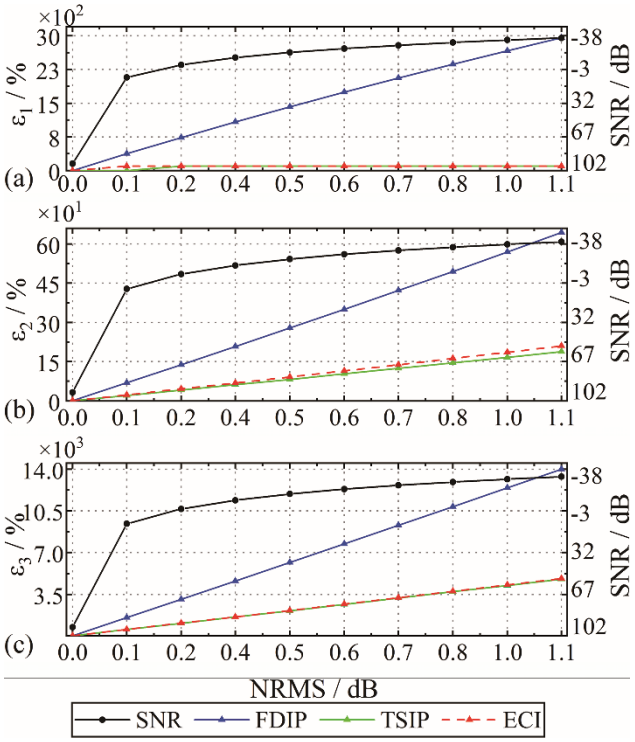

Figure 1. The effect of different degrees of Gaussian noise to the measures excitation signals in the phase-frequency characteristics. (a) SNR of the polluted potential signal. Complex resistivity relative error at (b) 80 Hz, (c) 160 Hz, (d) 320 Hz comparison using the three methods.

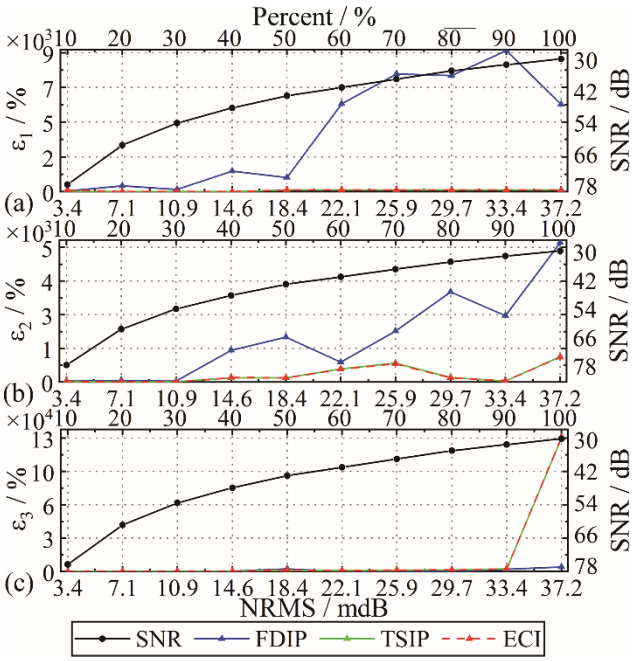

Figure 2. The effect of different levels of spike noises to the measured excitation signals. (a) SNR of the contaminated potential signal in the phase-frequency characteristics. Complex resistivity relative error at (b) 80 Hz, (c) 160 Hz, (d) 320 Hz comparison using the three methods.

From Figures 1 and 2, the results do not reflect the noise reduction performances of the three algorithms. Therefore, these results are not put into our manuscript. But |R(f)| and Phase(f) processed by three algorithms reflect their noise reduction performance well in the field experiment, as shown in Figure 3. So |R(f)| and Phase(f) in the field experiment are added to our manuscript.

This information is added on Page 9, line 16 and 17, Page 10, line 1 to 5 and Figure 3.

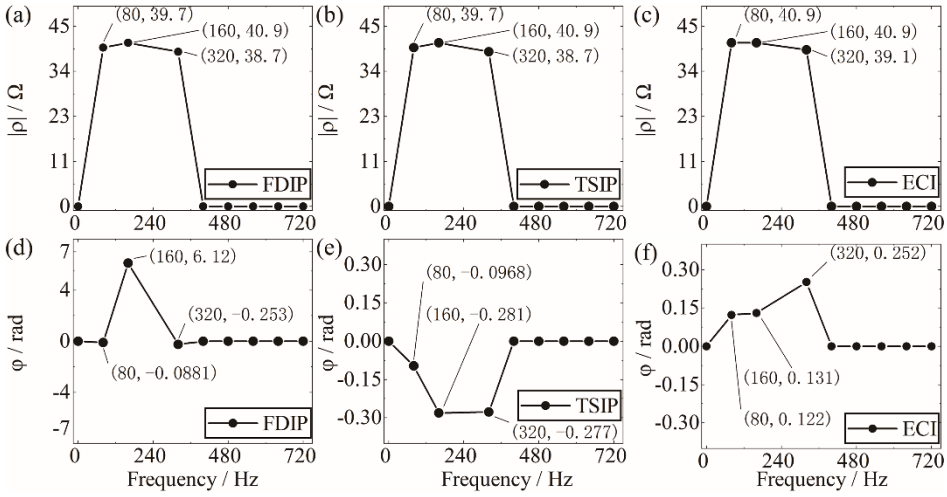

Figure 3. Complex resistivity spectrum calculated by the three algorithm (one period) in survey point No 21.

Comment 3. Page 7: “ECI algorithm still has superior denoising performance and holds smaller

volatility of the relative error when the percentage of the outliers is more significant than 50% .” What do you mean by volatility here? This sentence is unclear.

Response.

By ‘volatility’ we were trying to say ‘fluctuation’, sorry for causing misunderstanding.

Page 6, line 8

Comment 4. What situations would the algortim fail? That is, what are the limitations? Please show the limitations in detail (simulation or measured data and discussion).

Response.

In a real environment, this model is contaminated by the environment interference and measuring instrument. It can be categorized into three types: the Gaussian random noise, the impulse interference, and the particular frequency disturbance (Wang and Li, 1986; Yan et al., 2016).

For our system, we assume the three noises are linearly overlapping on the three sensors, along with some weak influence of coupling effects. So, the noises in the three sensors are only different in amplitude. Hence,

$$n_1(t) = B_1 g(t) + C_1 p(t) + D_1 s(t) \tag{1}$$

$$n_2(t) = B_2 g(t) + C_2 p(t) + D_2 s(t) \tag{2}$$

$$n_3(t) = B_3 g(t) + C_3 p(t) + D_3 s(t) \tag{3}$$

where $n_k(t)$ is the noise in sensor Y_k, $k = 1, 2, 3$, respectively. $g(t)$, $p(t)$ and $s(t)$ are separately Gaussian random noise, impulsive noise and particular frequency interference. B_k, C_k and D_k are the amplitudes of $g(t)$, $p(t)$ and $s(t)$, $k = 1, 2, 3$, respectively.

According to the properties of the correlation function, the cross-correlation results of the three kind of noise is as below:

A. For the Gaussian random noise, when $-NT \le \tau \le NT$ and $\tau \ne 0$, $R_{gg}(\tau)$ is shown in Figure 4.

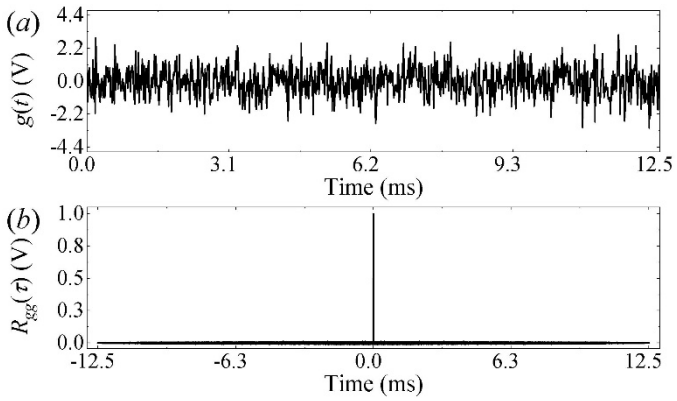

Figure 4. Waveform and autocorrelation for the Gaussian random noise $g(t)$. (a) its time domain waveform. (b) its autocorrelation $R_{gg}(\tau)$.

B. For the impulsive noise, when $-NT \le \tau \le NT$ and $\tau \ne 0$, it is considered that $R_{pp}(0) \gg R_{pp}(\tau)$, as shown in Figure 5.

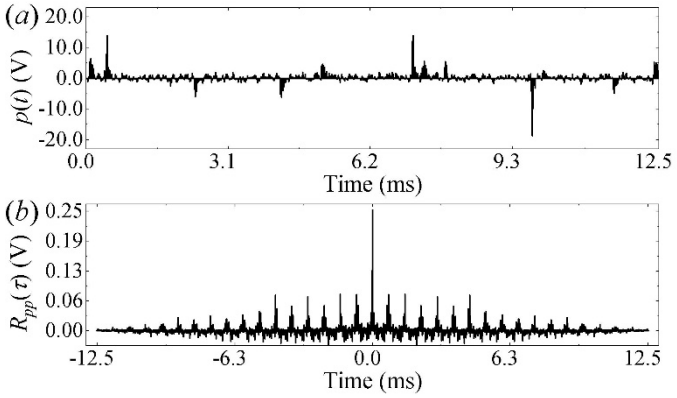

Figure 5. Waveform and autocorrelation for the impulsive noise $p(t)$. (a) its time domain waveform containing 20% of the outliers. (b) its autocorrelation $R_{pp}(\tau)$.

C. For the particular frequency disturbance, its autocorrelation has the same frequency with it, but when it is less effective for the transmitter output signal $u_{\mathrm{ab}}(t)$ than that of the $u_{\mathrm{mn}}(t)$ and $i(t)$, $D_1D_2R_{ss}(\tau)$ and $D_1D_3R_{ss}(\tau)$ can be effectively suppressed, as shown in Figure 6.

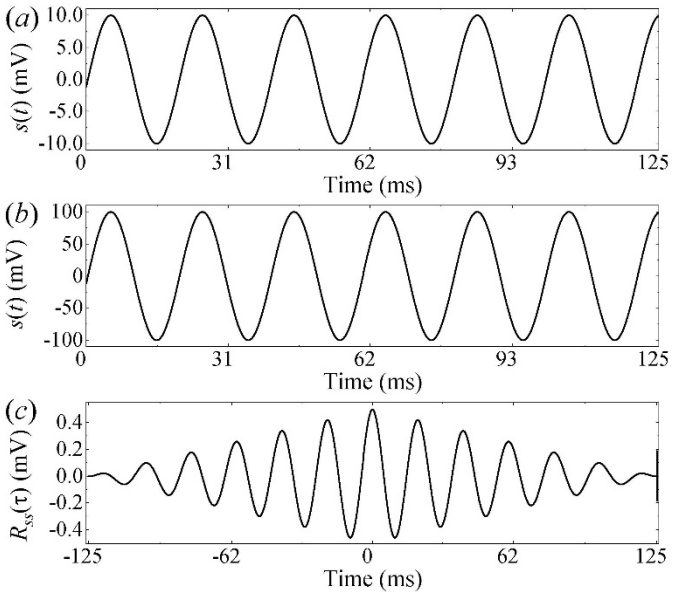

Figure 6. Waveform and autocorrelation for the particular frequency interference $s(t)$. The power-line interference (a) at $D_1 = 0.01$, (b) at $D_2 = 1$. (c) their cross-correlation $D_1 D_2 R_{ss}(\tau)$.

Based on the analysis above, it can be concluded that the influences of Gaussian random and impulsive noises are more effectively suppressed, while the particular frequency disturbance is attenuated to some degree when the noise is in lower intensity. Therefore, the proposed method has more value on denoising for Gaussian and impulsive random noises.

Page 10, line 15 and 16

References

Wang, F.S., and Li, T., 1986, Industry of stray current resistivity observation and avoid interference distance: Northeastern Seismological Research, 2, 44–48. doi:10.13693/j.cnki.cn21-1573.1986.02.006

Yan, T. J., Wang, S. Q., Mang, Y. X., and Luo, X. Z., 2016, Influence of human interference on application of electrical prospect-ing and corresponding anti–interference measures , Mineral Exploration, 7, 634–639. doi:10.3969/j.issn.1674-7801.2016.04.016

Comment 5. Phase (or quadradture component) results must be presented and discussed, oth-erwise we are not looking at the IP effects.

Response.

(1) The phase results for the inversion results given by Res2DInv software is shown as Figure 7. As we can see, this figure shows chaos information from the phase shift between $i(t)$ and $u(t)$ of the three methods. This is because the loss layer surrounding the shelter is very weak polarized, so the phase shift is very small, which cause the result easily contaminated by some random factors. Therefore, we have not figured out how to extract meaningful information out of the phase results, but it is possible that with proper strong-polarized experiment field there could be different results. We are eager to explore that in our next experiment plan.

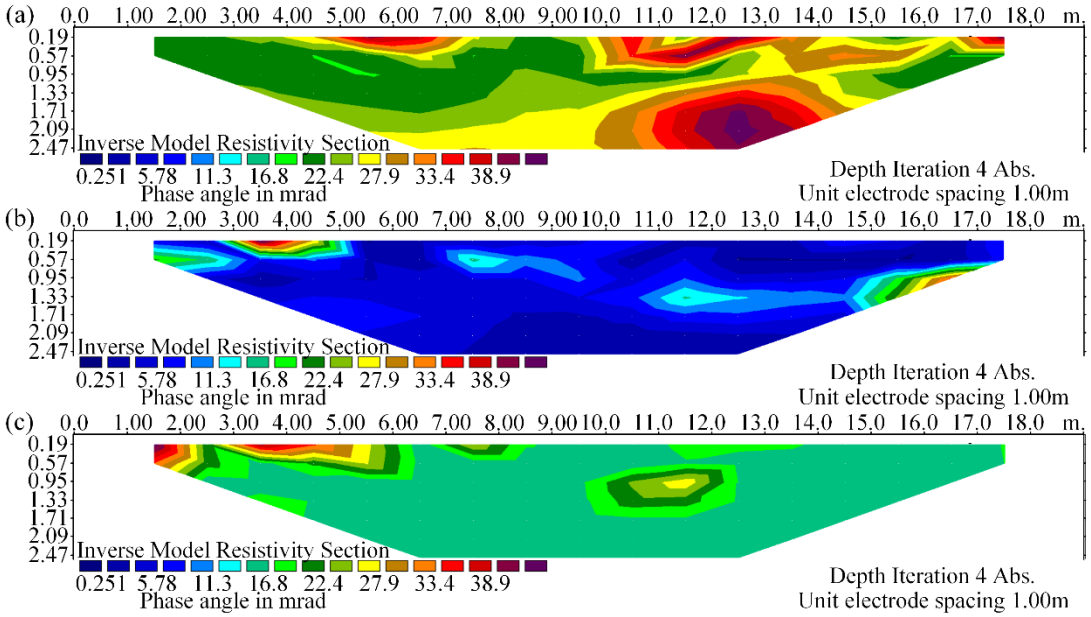

Figure 7. Inverted phase sections of the two high resistivity anomalies at 80Hz with using (a) the FDIP method, (b) the TSIP algorithm, and (c) the ECI algorithm.

(2) We added phase results to field experiment and not to simulation as we explained in Response 2.

An enhanced correlation identification algorithm and its application on spread spectrum induced polarization data

Siming He[1,2], Jian Guan[3], Xiu Ji[1], Hui Wang[1], and Yi Wang[2]

[1]School of Electrical and Information Engineering, Changchun Institute of Technology, Changchun 130000, China
[2]College of Instrumentation and Electrical Engineering, Jilin University, Changchun 130000, China
[3]College of Electronic Science & Engineering, Jilin University, Changchun 130000, China

Correspondence to: Yi Wang (e-mail: wangyijlu@jlu.edu.cn)

Abstract. In spread spectrum induced polarization (SSIP) data processing, attenuation of background noise from the observed data is the essential step that improves the signal-to-noise ratio (SNR) of SSIP data. The Time-Domain Spectral Induced Polarization Based on Pseudo-random Sequence (TSIP) algorithm has been proposed to improve the SNR of these data. However, signal processing in background noise is still a challenging problem. We propose an enhanced correlation identification (ECI) algorithm to attenuate the background noise. In this algorithm, the cross-correlation matching method is helpful for the extraction of useful components of the raw SSIP data and suppression of background noise. Then the frequency-domain IP (FDIP) method is used for extracting the frequency response of the observation system. Even when the signal to noise ratio (SNR) is -37.5dB, this ECI algorithm can still be able to keep 3.0% relative error. Experiments on both synthetic and real SSIP data show that the ECI algorithm can not only suppress the background noise but also better preserves the valid information of the raw SSIP data to display the actual location and shape of adjacent high resistivity anomalies, which can improve subsequent steps in SSIP data processing and imaging.

1 Introduction

Induced Polarization (IP) technology operated in both the time domain and the frequency domain is useful in exploration for groundwater mapping, mineral exploration, and other environmental studies (Revil 2012, 2019; Høyer et al. 2018). Since the phenomenon of IP in time domain was first discovered by Schlumberger in 1920s, there has been consistent efforts to explore its utilization in various researches. In 1959, the frequency-domain IP (FDIP) approach is proposed by Collett and Seigel, which became the most classic and widely used mapping technique. For example, the first variable-frequency approach was proposed by Wait et al in 1959, then the spectrum approach of the complex resistivity was developed by Zonge and Wynn in 1975, and the dual-frequency IP approach was presented and developed by He et al. in 1993 and Han et al. in 2013. Recently, spread spectrum induced polarization (SSIP) is a popular branch of FDIP which uses pseudo-random current pulses of opposite polarity as an excitation source (Chen et al., 2007; Xi et al., 2013, 2014; He et al. 2015). According to the intrinsic broadband characteristics of the source itself, the spectral response of an observation system can be simultaneously calculated at multiple frequencies in electrical exploration (Liu et al., 2019). Thus, this SSIP technology has been gaining attention and application in electrical prospecting (Xi et al., 2014; Lu et al., 2019; Wang and He, 2020).

SSIP technology has a certain degree of noise immunity, but it is still polluted by inevitable background noise in IP data acquisition. The background noise can be mainly categorized into two types: the Gaussian noise and the impulsive interference with different percentage of outliers (Liu et al., 2016; Kimiaefar et al., 2018; Li et al., 2019). If the background noise is not effectively reduced, the remnant noise can affect the calculation of complex resistivity and may mislead subsequent interpretations of the subsurface structure.

The field of FDIP denoising has achieved quite good results through the constant research of experts and scholars. There have been many algorithms that can be used to suppress the FDIP random noise (Mo et al., 2017), such as smooth filter (Guo, 2017), Mean stack (Liu, 2015), digital filter (Meng et al., 2015), and robust stacking (Liu et al., 2016). The smooth can effectively attenuate Gaussian noise, but the impulsive interference with intense energy leaves the effectiveness of this

algorithm limited. Therefore, an effective attenuative algorithm for background noise is still a challenging task for traditional noise suppression algorithms (Neelamani et al., 2008; Liu et al., 2017). SSIP method also faces the same issue (Liu et al., 2016, 2017).

Recently, the new algorithm based on a circular cross-correlation method, Time-Domain Spectral Induced Polarization Based on Pseudo-random Sequence (TSIP) algorithm, has also been used to suppress the SSIP noise (Li et al. 2013; Zhang et al. 2020). Due to its effective denoising ability, the identification method has gained more attention and development. However, the TSIP algorithm is restricted because the excitation signal is sensitive to the random noise. For this problem, we propose an enhanced correlation identification (ECI) algorithm for reducing the noise in SSIP data. The ECI algorithm obtains cross-correlations between the transmitter output signal, the excitation signal, and the response signal. The performance of the ECI algorithm is demonstrated on both synthetic and field SSIP data. Experimental results show that the ECI algorithm can effectively control the root mean square of noise (NRMS) increase, enhance its denoising performance in background noise and improve the valid signal preservation to display the actual location and shape of high resistivity anomalies with higher resolution.

2 Theory

2.1 Subsection (as Heading 2) The TSIP theoretical model

Figure 1 shows a traditional diagram of the electrical resistivity survey. The transmitter output signal $u_{\mathrm{T}}(t)$ is poured from electrode A to electrode B, the excitation signal $i(t)$ flows from electrode A to electrode B, and the response signal $u(t)$ between the electrodes M and N is measured. To simultaneously obtain the spectral response of subsurface at various frequencies, pseudo-random sequence based the excitation signal $i(t)$ is considered. Thus, the spectral response of subsurface be retrieved by the TSIP algorithm, and its spectral response be expressed as (Li et al., 2013):

$$H_e(\omega) = \frac{P_{ui}(\omega)}{P_{ii}(\omega) \cdot P_S(\omega)}, \tag{1}$$

where $P_{ui}(\omega)$ is the cross-power spectral density of $u(t)$ and $i(t)$, $P_{ii}(\omega)$ the auto-power spectral density of $i(t)$, and $H_S(\omega)$ is the impulse spectral response of the observing system.

Given this observation mode using low-power signals, the magnetotelluric system is a time-invariant system and let us suppose that $H_S(\omega)$ is 1. Eq. (1) can further be expressed as:

$$H_e(\omega) = \frac{P_{ui}(\omega)}{P_{ii}(\omega)} = \frac{fft[R_{ui}(\tau)]}{fft[R_{ii}(\tau)]} = \frac{U(\omega)}{I(\omega)}, \tag{2}$$

where $fft[.]$ denotes Fast Fourier Transform (FFT), , $R_{ui}(\tau)$ is the cross-correlation function of $u(t)$ and $i(t)$, $R_{ii}(\tau)$ is the auto-correlation function of $i(t)$, $U(\omega)$ and $I(\omega)$ depict the geometric factor defined by the frequency spectrum of $u(t)$ and the frequency spectrum of $i(t)$ respectively, and τ denotes time-delay.

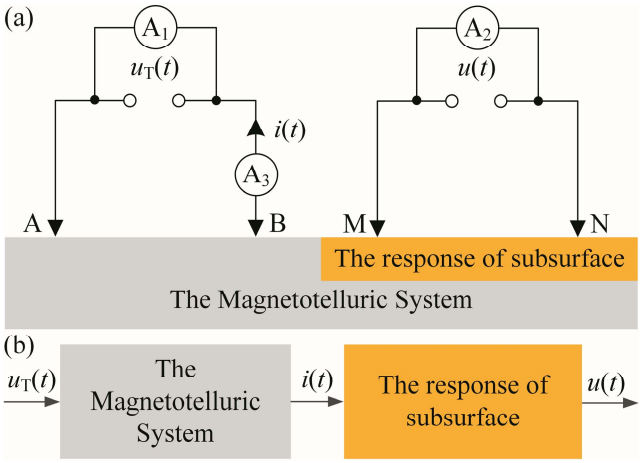

Figure 1. (a) The observation model of the four-electrode measurement. (b) its equivalent diagram.

In the practical field environment, this observation mode is contaminated by the background noise, as shown in Figure2. The output of the sensors A_k (k=1, 2, 3) can be expressed as:

$$y_1 = u_T(t) + n_1(t), \tag{3}$$

$$y_2 = u(t) + n_2(t), \tag{4}$$

$$y_3 = i(t) + n_3(t), \tag{5}$$

where $n_k(t)$ is the background noise.

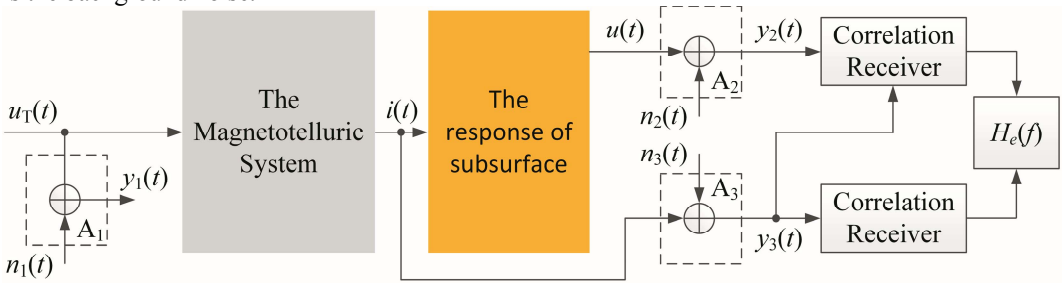

Figure 2. Schematic diagram using the TSIPD algorithm.

Therefore, according to Eq. (2), the formula of the TSIP algorithm is given as:

$$H_e(\omega) = \frac{P_{y_2y_3}(\omega)}{P_{y_3y_3}(\omega)} = \frac{fft[R_{y_2y_3}(\tau)]}{fft[R_{y_3y_3}(\tau)]} = \frac{fft[R_{ui}(\tau) + R_{un_2}(\tau) + R_{in_1}(\tau)]}{fft[R_{ii}(\tau) + R_{in_1}(\tau) + R_{n_1n_1}(\tau)]} \approx \frac{fft[R_{ui}(\tau)]}{fft[R_{ii}(\tau) + R_{n_3n_3}(\tau)]}. \tag{6}$$

Eq. (6) demonstrates that the TSIP algorithm has a weak denoising effect when $n_3(t)$ is the massive intense noise. In other words, the TSIP algorithm depends on the energy intensity of $n_3(t)$ present in $i(t)$.

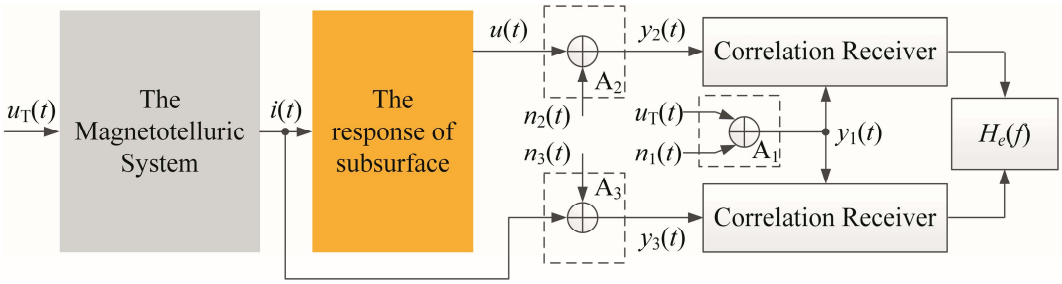

Figure 3. The schematic diagram of the ECI denoising model.

2.2 The ECI theoretical model

That the denoising ability of the TSIP algorithm is limited is caused by that $i(t)$ is sensitive to $n_3(t)$. To solve this problem, the ECI algorithm is proposed and its derivation process is as follows.

Firstly, let us suppose that the telluric system is a time-invariant system under low-power signals. For three sensor output signals, their cross-correlation functions are the periodic correlation functions of time τ. When the length of the correlation window NT is specified, 0.0125s in this experiment. The cross-correlation functions can be expressed as follows:

$$R_{y_1y_2}(\tau)=\mathrm{E}[y_1(t)y_2(t\text{-}\tau)]=(R_{u_Tu}(\tau))_N+R_{n_1n_2}(\tau), \tag{7}$$

$$R_{y_1y_3}(\tau)=\mathrm{E}[y_1(t)y_3(t\text{-}\tau)]=(R_{u_Ti}(\tau))_N+R_{n_1n_3}(\tau), \tag{8}$$

where $R_{n_1n_2}(\tau)$ and $R_{n_1n_3}(\tau)$ are the cross-correlations of, $n_2(t)$ and $n_3(t)$ respectively, and τ is time-delay that lies in the range of $-NT$ to NT.

According to the design features of ZW-CMDSII (Zhang, et al., 2014; He, et al., 2014;), $n_1(t)$ caused mainly by the floor noise energy of the instrument is relatively very low, while $n_2(t)$ and $n_3(t)$ possess much higher energy level because they are mainly composed of environment noise. Thus we can assume that the cross-relation between $n_1(t)$ and $n_2(t)$, $n_3(t)$, $R_{n_1n_2}(\tau)\approx 0$ and $R_{n_1n_3}(\tau)\approx 0$.

Based on the above analyses, we can further obtain:

$$R_{y_1y_2}(\tau)\approx(R_{u_Tu}(\tau))_N, \tag{9}$$

$$R_{y_1y_3}(\tau)\approx(R_{u_Ti}(\tau))_N. \tag{10}$$

Then the cross-power spectrum of Eq. (9) and Eq. (10) can be written as following

$$P_{y_1y_2}(\omega)\approx P_{u_Tu}(\omega), \tag{11}$$

$$P_{y_1y_3}(\omega)\approx P_{u_Ti}(\omega). \tag{12}$$

Finally, according to Eq. (2) and Eq. (11), Eq. (12) can be expressed as following

$$H_e(\omega)=\frac{U(\omega)}{I(\omega)}=\frac{U(\omega)U_T^*(\omega)}{I(\omega)U_T^*(\omega)}=\frac{P_{u_Tu}(\omega)}{P_{u_Ti}(\omega)}\approx\frac{P_{y_1y_2}(\omega)}{P_{y_1y_3}(\omega)}. \tag{13}$$

So, Eq. (13) is the formula of the ECI algorithm. The derivation process of this formula clearly describes that the ECI algorithm can effectively suppress the background noise and be independent on the degree of $n_3(t)$ present in $i(t)$.

3 Experiment on synthetic SSIP data record

We test the ECI algorithm for attenuating background noise of SSIP data sets in comparison with the FDIP algorithm and the TSIP algorithm. For the comparison, the SNR, root mean square of noise (NRMS) and relative error (ε) as the objective parameters to judge the performance of denoising, which are calculated as follows:

$$\mathrm{SNR} = 10\log_{10}\left\{\frac{\sum_{i=1}^{\mathrm{M}}[y(i)-\mu_y]^2}{\sum_{i=1}^{\mathrm{M}}[n(i)-\mu_n]^2}\right\}, \tag{14}$$

$$\mathrm{NRMS} = \sqrt{\frac{\sum_{i=1}^{\mathrm{M}}[n(i)]^2}{\mathrm{M}}}, \tag{15}$$

$$\varepsilon = 100\times\frac{\rho_1-\rho_0}{\rho_0}, \tag{16}$$

$$i(t)=u_i(t)\,/\,R_{\mathrm{S}} \tag{17}$$

where μ_y and μ_n denote the mean values of the useful signal and the noise separately. $y(i)$ and $n(i)$ are the useful signal and the noise separately, M is the length, ρ_0 denotes the complex resistivity calculated without noise, and ρ_1 is the complex resistivity calculated with the noise added to ρ_0. R_{S} is the value of the sampling resistor ($R_{\mathrm{S}}=1\Omega$), and $u_i(t)$ is the voltage at the sampling resistor.

To validate the effectiveness of the ECI algorithm, we test for one practically recorded data set. Firstly, we use the applied voltage $u_{\mathrm{T}}(t)$, the injected current $i(t)$ and the measured potential signal $u(t)$ as the raw signals. These signals are a 3-order spread spectrum pseudo-random sequence at the clock cycle of 0.0125s, as shown in Figures 4a-c. Secondly, In our experiment the measurement line is 19m and in a stable environment, so we consider the system linear time-invariant and the noise from the current and voltage measurement are linearly superpositioned (Pelton, et al., 1983; De, et al., 1983; Vinegar and Waxman, 1984; De, et al., 1992; Garrouch and Sharma, 1998). Therefore, it is actually equivalent whether the noise is added to the injected current $i(t)$, the measured potential signal $u(t)$ or the applied voltage $u_{\mathrm{T}}(t)$. Therefore, the injected current $i(t)$ is only polluted by the synthetic background noise, including Gaussian and impulsive, as shown in Figures 4d and e. Thirdly, the complex resistivity of the main frequency is considered and discussed because the main energy of the pseudo-random signal is concentrated on the main frequency (He, 2017). Finally, for detailed comparisons between the ECI algorithm and the others, we add the synthetic Gaussian and impulsive noises to the response signal $i(t)$, respectively.

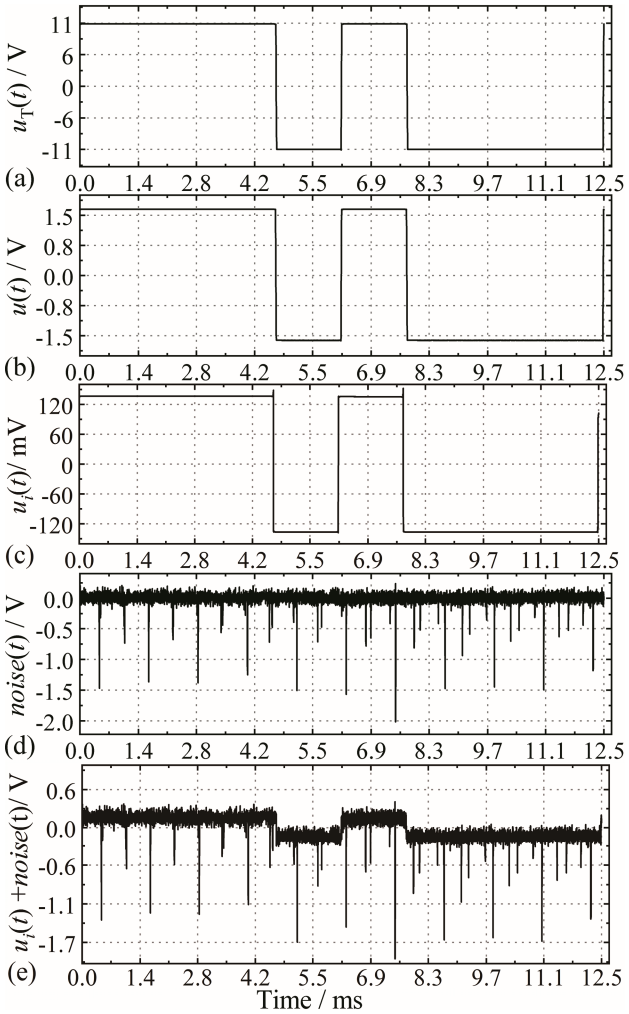

Figure 4. The time waves of (a) the applied voltage $u_T(t)$, (b) the measured potential signal u(t), (c) the voltage $u_i(t)$ at the sampling resistor, (d) noise(t), and (e) the synthetic signal ($u_i(t)$+ noise(t)).

We use synthetic Gaussian noise with the deviation and mean value of 0.1 and 1.1 as a standard template. The excitation signal $i(t)$ is polluted by synthetic different energy levels of the Gaussian noise, as shown in Figure 5. The denoised results obtained by the ECI algorithm and the others are shown in Figures 5a-c. These figures show that the relative error and SNR of the excitation signal $i(t)$ are calculated and compared at the three main frequencies when the noise RMS ranges from 0 to 0.9. From Figure 5b, it can be seen that the denoising ability of TSIP algorithm depends on the energy intensity of the noise presence in the excitation signal $i(t)$, consistent with the conclusion of Eq. (6). Meanwhile, Figure 5 indicates that the ECI algorithm possesses the best denoising performance under the same noise RMS and SNR. Particularly, when the SNR is -37.5 dB, this ECI algorithm is still able to keep 3.0% relative error at the primary frequency 160Hz.

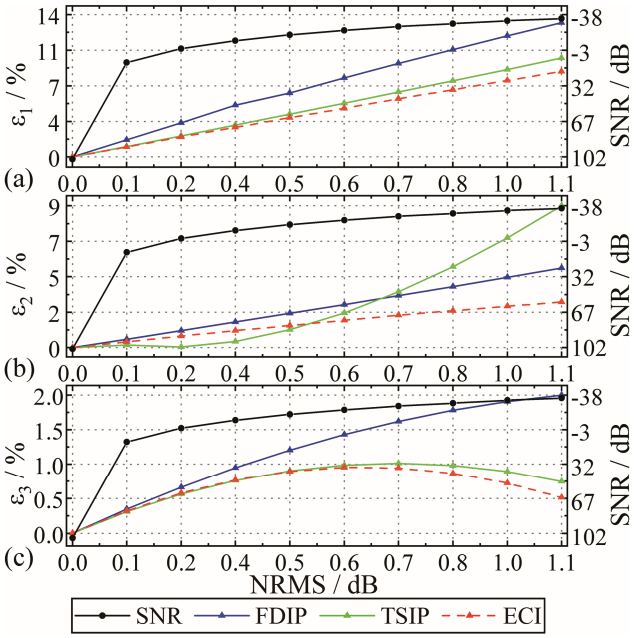

Figure 5. The effect of different degrees of Gaussian noise to the measures excitation signals. (a) SNR of the polluted potential signal. Complex resistivity relative error at (b) 80 Hz, (c) 160 Hz, (d) 320 Hz comparison using the three methods.

Previous literature has shown that if the percentages of outliers in impulsive noise exceed 50%, the traditional denoising algorithm will be limited (Liu et al., 2016, 2017). Thus, Synthetic impulsive noise is added to the excitation signal $i(t)$ in ten percent steps. Their standard deviations (SDs) and skewnesses (SKs) are shown in Figure 6. As depicted in Figures 7, the three algorithms have a certain degree of denoising performance versus the different percentages of the synthetic outliers against the raw data. However, the ECI algorithm still has superior denoising performance and holds smaller fluctuation of the relative error when the percentage of the outliers is more significant than 50%. For example, the average SD in ECI processing the SSIP data is 37% and 51% lower than the FDIP and TSIP respectively.

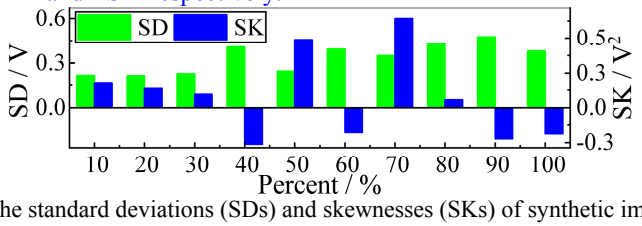

Figure 6. The standard deviations (SDs) and skewnesses (SKs) of synthetic impulsive noise.

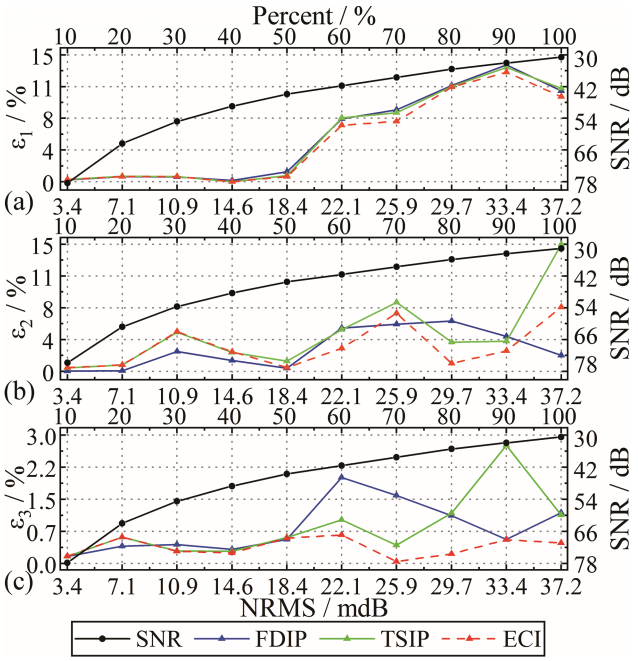

Figure 7. The effect of different levels of spike noises to the measured excitation signals. (a) SNR of the contaminated potential signal in the amplitude-frequency characteristics. Complex resistivity relative error at (b) 80 Hz, (c) 160 Hz, (d) 320 Hz comparison using the three methods.

4 Experiment on real SSIP data record

To further verify the performance of the ECI algorithm, the Wenner array, the traditionally applied system in the field, was selected for performing laboratory tests, as shown in Figure 8. SSIP data was acquired with high-density meter and 20 electrodes at 1m spacing. A Wenner acquisition sequence was adopted with 55 potential measurements expressed utilizing the green and points. The figure shows an example of two high resistance cavities. The two cavities were presented by the letters A and B, and their calibers were about 1.8 m × 2 m. The measured excitation signal had a range between 0.04 and 0.19 A approximately. The transmitter output signal is a three-order sequence with 80 Hz frequency, and its voltage is about ± 11.8 V. The sampling frequency is 625 kHz. The excitation and response data of 40 periods were recorded at each point.

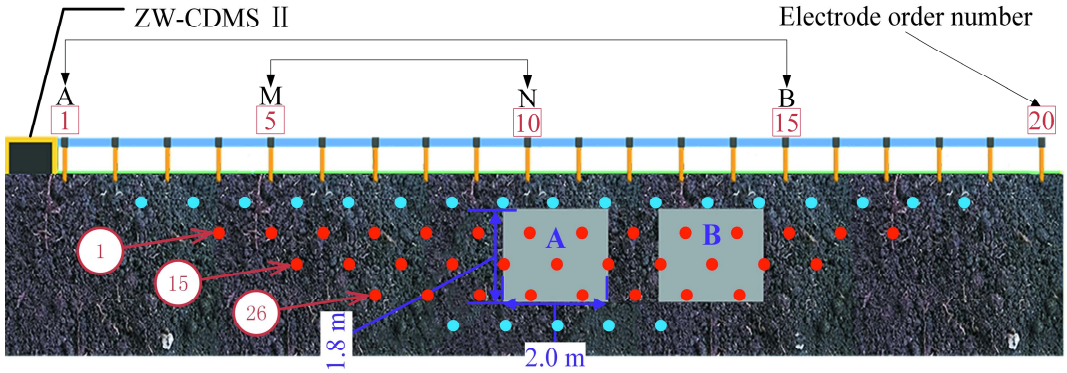

Figure 8. The schematic of the two high resistance cavities.

Figure 9 demonstrates the experimental SSIP data processed by the three algorithms, inverted with Res2DInv. It can be observed that the location and shape of two abnormal bodies are distinguished only in the ECI algorithm while recognized as one whole in the other algorithms. We believe the reason that ECI has higher detection precision is due to its higher denoising ability.

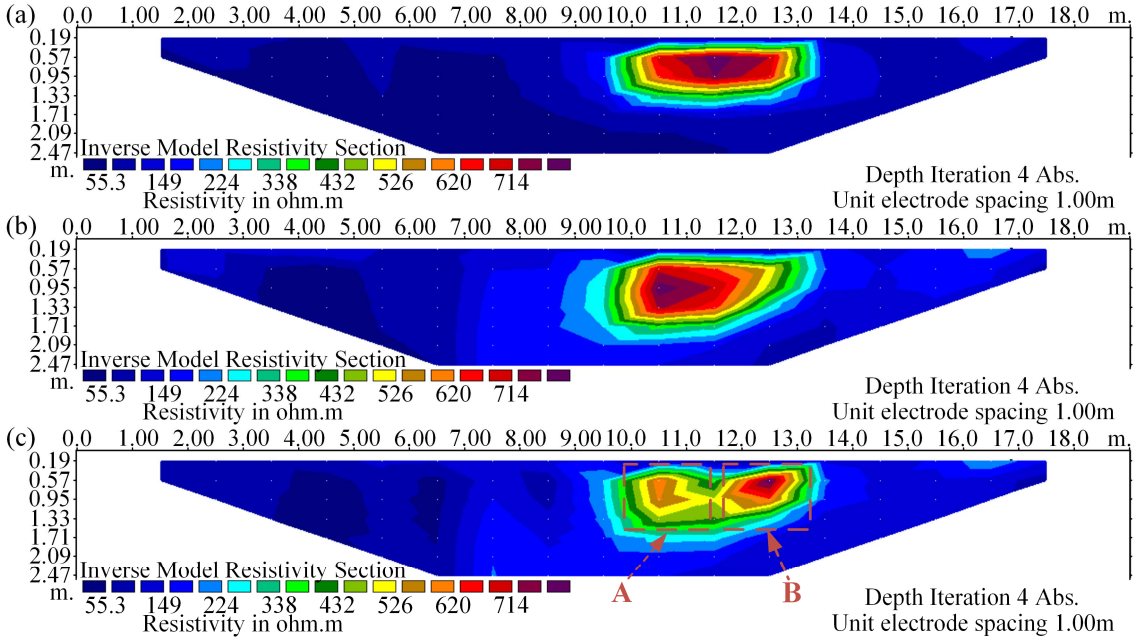

Figure 9. Inverted resistivity sections of the two high resistivity anomalies (A and B) at 80Hz with using (a) the FDIP method, (b) the TSIP algorithm, and (c) the ECI algorithm.

To verify the reason of the improved detecting precision, the SD for each red point is calculated, as shown in Figure 10. This figure shows that among the 33 SD of SSIP data by processed the ECI method is the lowest at all points except for the 28th. The average SD in ECI processing the SSIP data is 7% and 3.8% lower than the FDIP and TSIP respectively. Also, the maximum value of SDs with the ECI method is 5% and 1.4% lower than the others, and the minimum value is 8% and 10% lower, respectively. The These results quantitively indicate that the ECI algorithm improves the accuracy and robustness of the collected data.

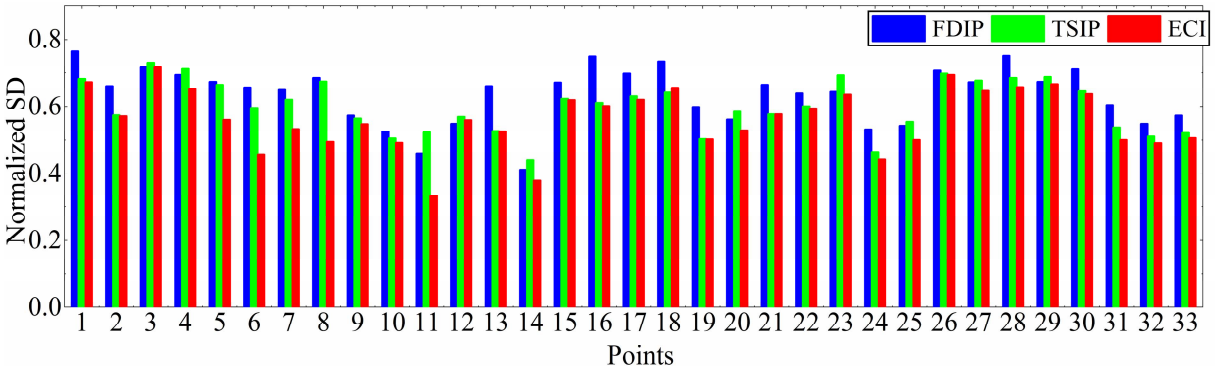

Figure 10. Standard deviation (SD) of the ECI algorithm and the others to the red data dots at 80Hz.

Meanwhile, amplitude-frequency $|\rho(f)|$ and phase-frequency $\varphi(f)$ characteristics of complex resistivity are calculated by the three algorithm (one period) in survey point No 21, in Figure 11. As depicted in Figure 11, the complex resistivity processed

by the ECI shows a linear trend with the three main frequencies. Also, the SD of the amplitude-frequency $|\rho(f)|$ characteristic is 9.9% and 4.9% lower than the others, and the SD of the phase-frequency $\varphi(f)$ is 356.1% and 3.3% lower. Therefore, we believe that the ECI algorithm has advantage on suppressing background noise, which benefits the subsequent steps in SSIP data processing and imaging.

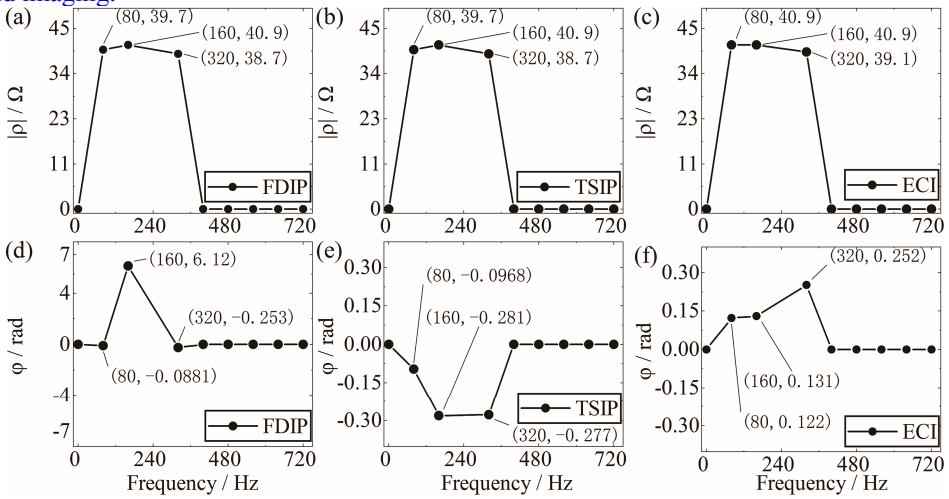

Figure 11. Complex resistivity spectrum calculated by the three algorithm (one period) in survey point No 21.

5 Conclusions

We propose the ECI algorithm that effectively attenuates the background noise in SSIP data and improves the complex resistivity spectrum. This method uses the correlation function to neutralize the influence of the background noise in the SSIP data, and the spectrum complex resistivity can be calculated at multiple frequencies by the formula of the complex resistivity. Simulation results show that the ECI algorithm can effectively attenuate the background noise and improve the SNR. Subsequently, the practicability of the ECI algorithm is further verified by a field test. The results demonstrate that the SD of the SSIP data is improved, which benefits the accuracy and stability of the collected data. There is a good agreement between the complex resistivity and the geological target body with high resistance, which indicates that the ECI algorithm can help to improve the quality of interpretation and inversion in the survey area. The ECI algorithm can more effectively suppress the background noise including the Gaussian random and impulsive noises, but its effect on particular frequency disturbance is very limited due to the periodicity of the disturbance. Therefore, denoising algorithm based on pseudo random sequence correlation identification is still left open for more investigation.

References

Chen, R. J., Luo, W. B. and He,J. S.: High precision multi-frequency multi-function receiver for electrical exploration, 8th International Conference on Electronic Measurement and Instruments (ICEMI'07), IEEE, Expanded Abstracts, 599–602, https://doi.org/10.1109/icemi.2007.4350521, 2007.

Collett, L. S.: Laboratory investigation of overvoltage, in J. R. Wait, ed., Overvoltage research and geophysical applications, International series of monographs on earth sciences. Pergamon, New York, 50–70, https://doi.org/10.1016/b978-0-08-009272-0.50009-1, 1959.

De Lima, O. A. L., and Sharma, M. M.: A generalized Maxwell - Wagner theory for membrane polarization in shaly sands: Geophysics, 1992, 57, 431-440. doi:10.1190/1.1443257

Garrouch, A. A., Sharma M. M.: Dielectric dispersion of partially saturated porous media in the frequency range 10 Hz to 10 MHz: The Log Analyst, 1998, 39, 48-53.

Guo, H.: Study of key technology and data fusion of multi-probe penetration based on gas hydrate exploration, PhD. Thesis, China University of Geosciences, Wuhan, 2017.

Han, S. L., Zhang, S. G. Liu, J. X. H. Hu, J. and Zhang, W. S.: Integrated interpretation of dual frequency induced polarization measurement based on wavelet analysis and metal factor methods, Transactions of Nonferrous Metals Society of China, 23, 1465–1471, https://doi.org/10.1016/S1003-6326(13)62618-7, 2013.

He, G.: Wide area electromagnetic method and pseudo random signal method. Higher Education Press, 2017.

He, G. Wang, J. Zhang, B. Y. Li, M. and Ma, C.: Design of High-density Electrical Method Data Acquisition System, Instrument Technique and Sensor, 2014, 8, 18-19, https:// doi.org/10.3969/j.issn.1002-1841.2014.08.007.

He, J. H. Yang, Y. Li, D. Q. and Weng, J. B.: Wide field electromagnetic sounding methods, In Symposium on the Application of Geophysics to Engineering and Environmental Problems (SAGEEP 2015), EEGS, Expanded Abstracts, 325-329. https://doi.org/10.4133/sageep.28-047. 2015.

He, J. S.: Dual-frequency IP, Transactions of Nonferrous Metals Society of China-English edition, 3, 1–10, 1993.

Kimiaefar, R. Siahkoohi, S.H. Hajian, A. and Kalhor, A.: Random noise attenuation by Wiener-ANFIS filtering, J. Appl. Geophys., 159, 453–459. https://doi.org/10.1016/j.jappgeo.2018.05.017, 2018.

Li, G. Liu, X. Tang, J. Li, J. Ren, Z. and Chen, C.: De-noising low-frequency magnetotelluric data using mathematical morphology filtering and sparse representation, J. Appl. Geophys., 172, 103919. https://doi.org/10.1016/j.jappgeo.2019.103919, 2019.

Li, M. Wei, W. Luo, W. and Xu, Q: Time-domain spectral induced polarization based on pseudo-random sequence, Pure and Applied Geophysics, 170(12), 2257-2262, https:// doi.org/10.1007/s00024-012-0624-z, 2013.

Liu, N.: Preprocessing and Research of denosing methods for marine controlled source electromangnetic data, Msc. Thesis, Jilin University, Jilin, 2015.

Liu, W. Q. and Chen, R. J.: Coherence analysis for multi-frequency induced polarization signal processingin strong interference environment, The Chinese Journal of Nonferrous Metals (in Chinese), 26(3), 655–665. https://doi.org/10.19476/j.ysxb.1004.0609.2016.03.022, 2016.

Liu, W. Q. Chen, R. J. Cai, H. Z. and Luo, W. B.: Robust statistical methods for impulse noise suppressing of spread spectrum induced polarization data, with application to a mine site, Gansu province, China, J. Appl. Geophys., 135, 397–407. https://doi.org/10.1016/j.jappgeo.2016.04.020, 2016.

Liu, W. Q. Chen, R. J. Cai, H. Z. Luo, W. B. and Revil, André.: Correlation analysis for spread spectrum induced polarization signal processing in electromagnetically noisy environments, Geophysics, 82(5), E243–E256. https://doi.org/10.1190/geo2016-0109.1, 2017.

Liu, W. Q. Lü, Q. Chen, R. Lin, P. Chen, C. Yang, L. and Cai, H.: A modified empirical mode decomposition method for multiperiod time-series detrending and the application in full-waveform induced polarization data, J. Appl. Geophys., 217(2), 1058–1079. https://doi.org/10.1093/gji/ggz067, 2019.

Liu, W. Q. Wang, J. L. and Lin, P. R.: Signal processing approaches to obtain complex resistivity and phase at multiple frequencies for the electrical exploration method, Bollettino di geofisica teorica ed applicate, 58(2), 103–114. https://doi.org/10.4430/bgta0190, 2017.

Liu, W. Q. Lü, Q. T. Chen, R. J. Lin, P. R. Chen, C. J. Yang, L. Y. and Cai, H. Z.: A modified empirical mode decomposition method for multiperiod time-series detrending and the application in full-waveform induced polarization data, Geophysical Journal International, 217(2), 1058–1079. https://doi.org/10.1093/gji/ggz067, 2019.

Lu, Q. T. Zhang, X. P. Tang, J. T. Jin, S. Liang, L. Z. N, J. J. Wang, X. B. Lin, P. R. Yao, C. L. Gao, W. l. Gu, J. S. Han, L. G. Cai, Y. Z. Zhang, J. C. liu, B. L. and Zhao, J. H.: Review on advancement in technology and equipment of geophysical exploration for metallic deposits in china, Chinese J. Geophys. (in Chinese), 62(10), 3629−3664, https://doi.org /10.6038/cjg2019N0056, 2019.

Neelamani, R. Baumstein, A.I. Gillard, D.G. Hadidi, M.T. and Soroka, W.L.: Coherent and random noise attenuation using the curvelet transform, The Leading Edge, 27(2), 240–248. https://doi.org/10.1190/1.2840373, 2008.

Meng, Q. X. Pan, H. P. and Luo, M.: A study on the discrete image method for calculation of transient electromagnetic fields in geological media, Applied Geophysics, 2015, 12(4), 493–502. https://doi.org/10.1007/s11770-015-0517-x.

Mo, D. Jiang, Q. Y. Li, D. Q. Chen, C. J. Zhang, B. M. and Liu, J. W.: Controlled-source electromagnetic data processing based on gray system theory and robust estimation, Applied Geophysics, 14(4), 570–580. https://doi.org/10.1007/s11770-017-0646-5, 2017.

Wang, Y. B. and He, J. S.: A hybrid coding and its application to the oil and gas fracturing intelligent real time monitoring system based on pseudorandom signal, Geophysical and Geochemical Exploration, 44(1), 74−80, https://doi.org /10.11720 /wtyht.2020.2288, 2020.

Wait, J. R.: The variable-frequency method, in J. R. Wait, ed., Overvoltage research and geophysical applications: Pergamon, International series of monographs on earth sciences, 29–49, http://doi.org /10.1016/b978-0-08-009272-0.50008-x, 1959.

Pelton, W. H., and Sill, W. R.: Interpretation of complex resistivity and dielectric data: Geophysical Transactions, 1983, 29, 297-330.

Revil, A. Karaoulis, M. Johnson, T. and Kemna, A.: Review: Some low-frequency electrical methods for subsurface characterization and monitoring in hydrogeology, Hydrogeology Journal, 20, 617-658, https://doi.org /10.1007/s10040-011-0819-x 2012.

Revil, A. Razdan, M. Julien, S. Coperey, A, Abdulsamad, F. Ghorbani, A. and Rossi, M.: Induced polarization response of porous media with metallic particles — Part 9: Influence of permafrost, Geophysics, 84, E337–E355. https://doi.org /10.1190/geo2019-0013.1, 2019.

Xi, X. L. Yang, H. C. He, L. F. and Chen, R. J.: Chromite mapping using induced polarization method based on spread spectrum technology, Symposium on the Application of Geophysics to Engineering and Environmental Problems (SAGEEP 2013), EEGS, Expanded Abstracts, 13–19, https://doi.org/10.4133/sageep2013-015.1, 2013.

Xi, X. L., Yang, H. C. Zhao, X. F. Yao, H. C. Qiu, J. T. Shen, R. J. and Chen, R. J.: Large-scale distributed 2D/3D FDIP system based on ZigBee network and GPS, Symposium on the Application of Geophysics to Engineering and Environmental Problems (SAGEEP 2014), EEGS, Expanded Abstracts, 130–139, https://doi.org /10.1190/SAGEEP.27-055, 2014.

Schlumberger, C.: Study of underground electrical prospecting, Paris, 99, 1920.

Seigel, H. O.: Mathematical formulation and type curves for induced polarization, Geophysics, 24, 547–565, https://doi.org /10.1190/1.1438625, 1959.

Vinegar, H. J., and Waxman, M. H.: Induced polarization of shaly sands: Geophysics, 1984, 49, 1267–1287. doi:10.1190/1.1441755

Zhang, B. Y. He, G. and Wang J.: New High-density Electrical Instrument Measuring System. Instrument Technique and Sensor, 2014, 1, https://doi.org /10.3969/j.issn.1002-1841.2014.01.009.

Zhang, Q. D. Hao, K.X. and Li, M.: Improved correlation identification of subsurface using all phase FFT algorithm, KSII Transactions on Internet & Information Systems, 14(2), 495-513.19p, 2020.

Zonge, K. L. and Wynn, J. C.: Recent advances and applications in complex resistivity measurements, Geophysics, 40, 851–864, https://doi.org /10.1190/1.1440572, 1975.